Enthalpy-Entropy Compensation Effect for Triplet Pair Dissociation of Intramolecular Singlet Fission in Phenylene Spacer-bridged Hexacene Dimers

Shunta Nakamura,[†] *Hayato Sakai,*[†] *Masaaki Fuki,*[§,◊] *Yasuhiro Kobori,**[§,◊], *Nikolai V. Tkachenko**[,‡] *and Taku Hasobe**[,†]

[†]Department of Chemistry, Faculty of Science and Technology, Keio University, Yokohama, Kanagawa 223-8522, Japan

[§]Molecular Photoscience Research Center, Kobe University, 1-1 Rokkodai-cho, Nada-ku, Kobe 657-8501, Japan

[◊]Department of Chemistry, Graduate School of Science, Kobe University, 1-1, Rokkodai-cho, Nada-ku, Kobe 657-8501, Japan

[‡]Faculty of Engineering and Natural Sciences, Tampere University, P.O. Box 541, 33101 Tampere, Finland

Corresponding Author

*E-mail: hasobe@chem.keio.ac.jp (T.H.).

*E-mail: nikolai.tkachenko@tuni.fi (N.T.).

*E-mail: ykobori@kitty.kobe-u.ac.jp (Y.K.).

ABSTRACT. Hexacene (Hc) is highly promising for singlet fission (SF). However, the number of SF in Hc is extremely limited. As far as Hc dimers in solution are concerned, there is no report on the observation of the dissociation process from a correlated triplet pair (TT) to individual one. The emphasis in this study is on the first observation of the quantitative TT generation together with the orientation-dependent photophysical discussions for TT dissociation using *para*- and *meta*-phenyl-bridged Hc dimers. Moreover, the activation enthalpies of Hc dimers in TT dissociation are smaller than those of pentacene (Pc) dimers, whereas the relative entropic contributions for Gibbs free energy of activation are much larger than the enthalpic ones in both Hc and Pc dimers. This implies that the vibration motions are responsible for intramolecular conformation changes associated with TT dissociation. Consequently, 'enthalpy-entropy compensation' has a large effect on the rate constants and quantum yields.

TOC GRAPHICS

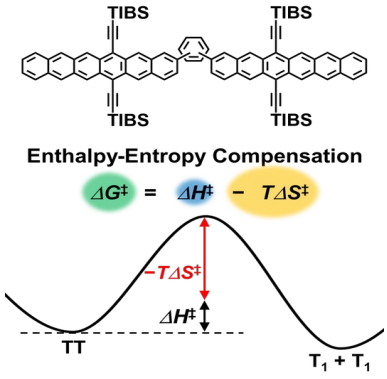

KEYWORDS: hexacene, molecular dimers, singlet fission, enthalpy-entropy compensation

Singlet fission (SF) is a spin-allowed multiexciton generation process, which is able to generate two individual triplet excitons (T_1+T_1) from one-photon absorption in two neighboring chromophores (S_0+S_1) (eq. 1).[1-3]

$$S_0 + S_1 \rightarrow TT \rightarrow T_1 + T_1 \qquad (1)$$

Where TT is a correlated triplet pair state. To efficiently perform SF, the energy level matching between the lowest-lying singlet excited state [$E(S_1)$] and two triplet excited states [$E(T_1)$] [that is, $E(S_1) \geq 2E(T_1)$] is required.[1] Among polyacenes, pentacene (Pc) sufficiently meets the above condition [$E(S_1)$: 1.83 eV and $E(T_1)$: 0.86 eV, $-{}^{o}G_{SF}$ = 0.11 eV].[4] Although SF was originally observed in thin films and single crystals composed of Pc and other molecules,[5-7] the quantitative TT generations are recently achieved in covalently-linked dimers[8-11] and related mesoscopic supramolecular assemblies[12-16] in addition to the important insights into SF mechanisms.[17-19] Although the photophysical discussions regarding the dissociation process from TT to T_1+T_1 were widely performed, the detail contributions of the enthalpic and entropic effects on the dissociation process (i.e., enthalpy-entropy compensation[20-24]) for Gibbs free energy of activation ($^{o}G^{\ddagger}$) has yet to be reported, so far.

Hexacene (Hc) is also one of the acene derivatives. Considering the above-mentioned energy matching condition between $E(S_1)$: 1.48 eV and $E(T_1)$: 0.44 eV,[25] the exothermic trend of Hc ($-{}^{o}G_{SF}$ = 0.60 eV) is evidently superior to Pc. The origin of the significant exothermicity in Hc is highly relevant with the high open-shell character.[26,27] High open-shell character induces a highly broken symmetry singlet state and stabilizes the corresponding triplet excited state.[28,29] Thus, the detailed evaluation of SF in Hc is quite interesting. However, in addition to the limited number of SF in Hc solid states,[25,30,31] only one example has focused on the ultrafast intramolecular SF process ($S_1S_0 \rightarrow$ TT) in a directly bridged-Hc dimer at 2 and 2' positions.[32] In

contrast, there is no report on the evaluation of the dissociation process (TT → T_1+T_1) of Hc dimers. Additionally, no attempt has been made to perform the systematic synthesis and photophysical evaluation of covalently-linked Hc dimers with different spacer units.

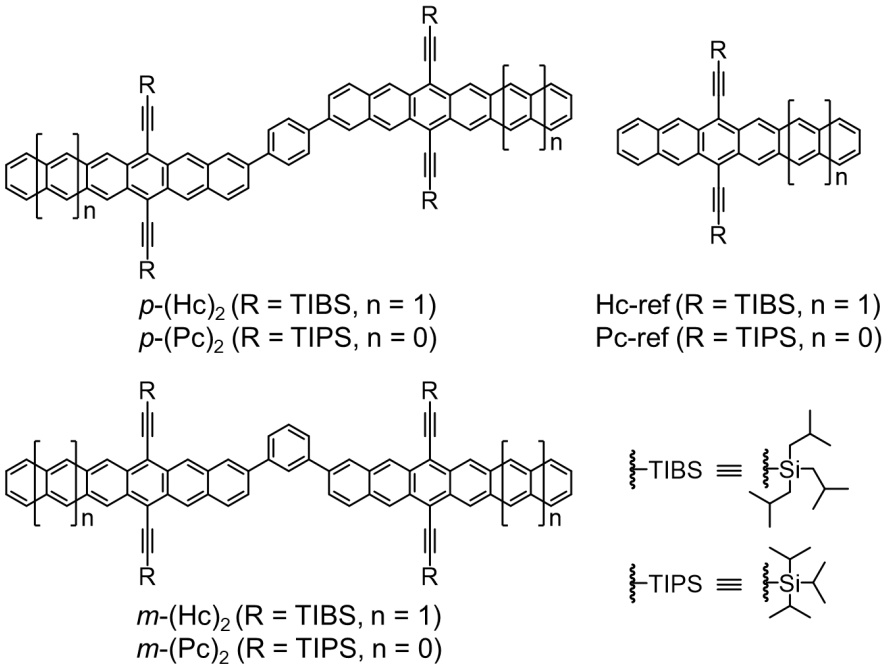

Figure 1. Chemical structures of Hc dimers and reference compounds in this study.

Based on the above points, we newly designed and synthesized Hc dimers linked by a phenylene spacer at *meta* and *para* positions (Figure 1) to focus on the intramolecular SF (ISF), especially the dissociation process from TT to T_1+T_1. Note that intramolecular electronic coupling is highly expected to be associated with the orientation of two chromophores (i.e., *meta*- or *para*-position in a phenylene unit) according to the previous reports.[10,33] The photophysical parameters of Hc dimers were largely different from those of Pc dimers. The activation enthalpies of Hc dimers in the dissociation process are smaller than those of Pc

dimers, whereas the relative entropic contributions for $^{o}G^{\ddagger}$ are much larger than the enthalpic ones in both Hc and Pc dimers. Consequently, the small differences of $^{o}G^{\ddagger}$ values between Hc and Pc dimers have a significant effect on the rate constants and quantum yields of the dissociation process (i.e., T_1+T_1 generation).

The details of synthetic procedures and characterizations of Hc dimers are described in Supporting Information (SI) (Scheme S1, Figures S1-S6 and Experimental Section in SI) together with Hc-ref[34] and Pc derivatives.[9,33] To discuss the electronic structures, firstly, absorption and fluorescence spectra were measured (Figures S7 in SI). The broadened and redshifted spectra of Hc dimers were observed as compared with Hc-ref. To compare the electronic coupling, DFT calculations were also performed (Figures S8-S9 and Tables S1-S3 in SI).[35,36] The results of DFT calculations suggest the strong electronic coupling of *p*-$(Hc)_2$ as compared to *m*-$(Hc)_2$ as described in SI (Figure S8 and Tables S1-S2 in SI). Moreover, the electronic couplings of Hc dimers are weaker than those of Pc dimers as described in SI (Figure S9 and Table S3 in SI) as rationalized by the reduced electron densities in the HOMO and LUMO orbitals at the carbons (C1, C2 and C3) in the phenylene spacers with respect to the densities at the corresponding carbons in the Pc dimers in Table S3 in SI.

To evaluate the ISF dynamics, femtosecond transient absorption (fsTA) spectra were measured using 100 fs laser pulses at 700 nm in toluene (Figure 2 and Figures S10-S11 in SI). First, triplet-triplet (T-T) absorption spectra of these three Hc derivatives were separately assigned and the corresponding molar absorption coefficients of T-T absorption (ε_T) were determined for the quantitative evaluation of individual triplet yields (Φ_T) (Figures S12-S14, Tables S4-S10 in SI). Typically, at few nanoseconds after excitation relatively narrow absorption bands with maxima at ca. 570 nm were observed and assigned to the T-T absorption. Broad

singlet-singlet (S-S) absorption bands with maxima at ca. 550 nm were observed virtually after excitation and also confirmed to be the singlet excited state comparing with Hc-ref in Figure S10 in SI. The rate constant of intersystem crossing: ISC (k_{ISC}) of Hc-ref was determined to be 2.5×10^6 s^{-1} (Figure S10 and detailed calculation process in SI). Figure 2A shows fsTA spectra of *p*-$(Hc)_2$. Shortly after laser-pulse excitation (ca. 1 ps), we can see broad TA spectra with an absorption maximum at ca. 550 nm, which is attributable to the S-S absorption (Figure 2B: black line). Then, new absorption bands appeared at ca. 120 ps. These absorption bands with the maximum at ca. 570 nm agree well with the above-mentioned T-T absorption of Hc unit (Figure 2B: blue and red lines). In *m*-$(Hc)_2$, the similar spectral trends were observed (Figure S11 in SI). Such a fast S-T conversion suggests a progression of ISF. Moreover, to obtain the direct evidences of the multiexcitons in *m*-$(Hc)_2$ in eq. (1), the strongly coupled quintet state ^{5}(TT) and the weakly coupled spin-correlated triplet pair (SCTP) of the intramolecular T+T state were both observed by the time-resolved electron paramagnetic resonance (TREPR) as shown in Figure S15 in SI. The electron spin polarization was explained by the spin polarization transfer model invoking conformation dynamics after the intramolecular SF using Eqs. (S1)-(S8) and Tables S11-S13 in SI.[37] Note that the non-zero J also excludes the triplet-isolation scenario via ^{3}TT → TS_0 annihilation in the present system. We can thus propose a kinetic model for ISF (Figure S16 in SI). To carefully discuss these kinetic processes, we analysed the species-associated spectra (SAS) of fsTA in *p*-$(Hc)_2$ (Figure 2C) together with the other Hc derivatives (Figures S10C and S11C in SI). SAS were obtained as a result of target analysis.[38,39] The rate constants of TT generation (S_1S_0 → TT) process (k_{TT}) and deactivation process from S_1 (k_S) were calculated by target analysis of fsTA (Table 1, Table S11 and Figure S16 in SI). The rate constants of TT generation (k_{TT}) were determined to be 2.1×10^{10} s^{-1} for *p*-$(Hc)_2$ and 4.5×10^8 s^{-1} for *m*-$(Hc)_2$,

respectively. These k_{TT} were several orders magnitude greater than the corresponding k_{ISC} [2.5×10^6 s^{-1} (see: Table 1)]. The k_{TT} of *p*-$(Hc)_2$ is two orders of magnitude greater than that of *m*-$(Hc)_2$. This is probably due to the electronic coupling between Hc units (*vide supra*). By utilizing the above mentioned k_{TT} and k_S, the Φ_{TT} of *p*-(Hc) and *m*-$(Hc)_2$ (maximum Φ_{TT}: 100%) were quantitatively determined to be 100% and 43%, respectively.

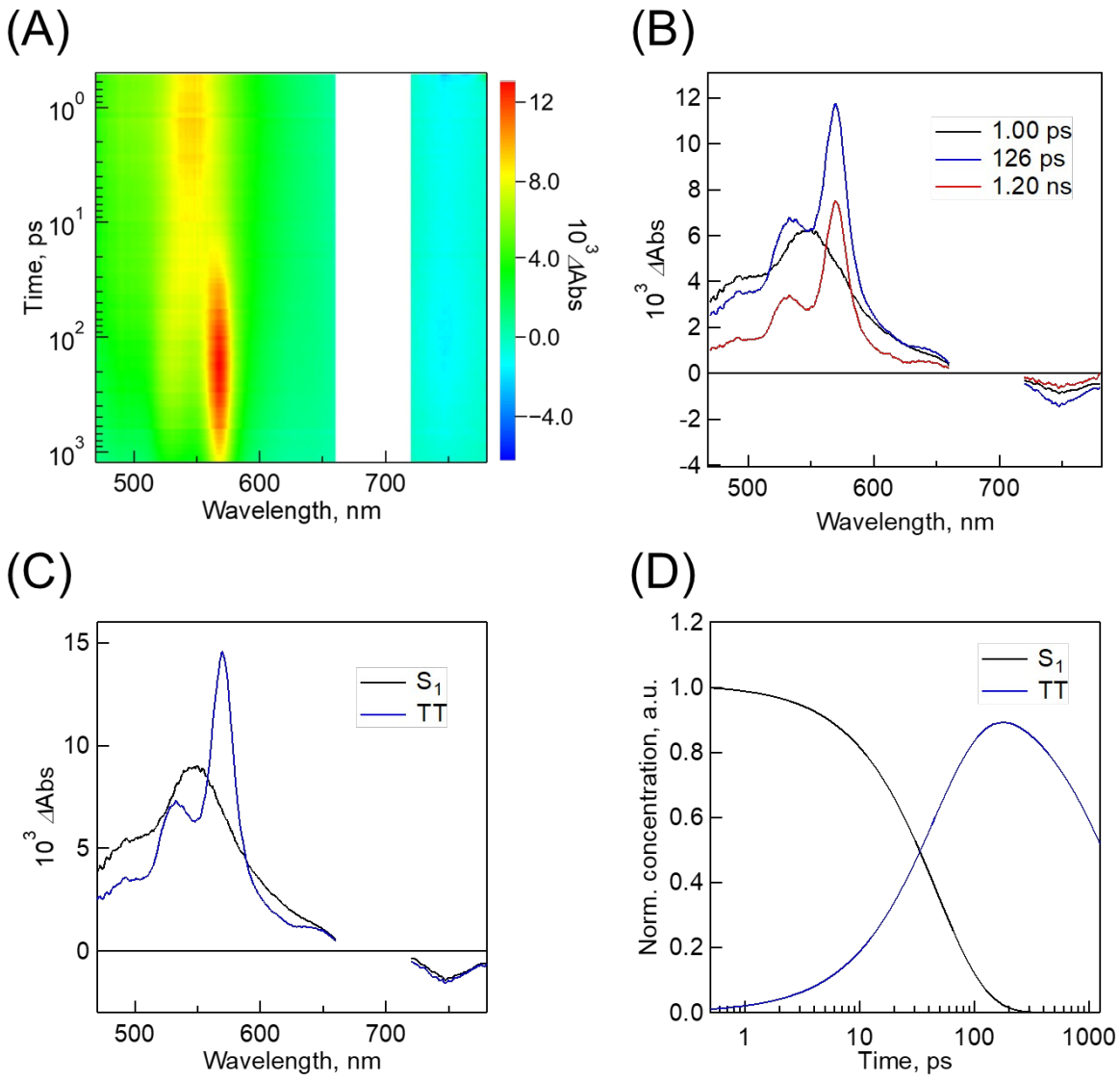

Figure 2. (A) fsTA spectra of *p*-$(Hc)_2$ in toluene (λ_{ex} = 700 nm). (B) Time-resolved spectra of *p*-$(Hc)_2$ at different time. (C) The species-associated spectra of *p*-$(Hc)_2$: S_1 (black line) and TT (blue line). (D) Time-dependent concentration profiles of S_1 (black line) and TT (blue line) of *p*-$(Hc)_2$.

Based on the above discussions, we have successfully observed high-yield TT generation in *p*-$(Hc)_2$. Similarly, the kinetic values of *p*-$(Pc)_2$ and *m*-$(Pc)_2$ reported by our group[10,33] were shown in Table 1. In the case of comparison between Hc and Pc dimers, the k_{TT} of *p*-$(Pc)_2$ (8.5×10^{10} s^{-1}) is somewhat larger than that of *p*-$(Hc)_2$ (2.1×10^{10} s^{-1}), which is similar to the relation between *m*-$(Pc)_2$ (2.1×10^{9} s^{-1}) and *m*-$(Hc)_2$ (4.5×10^{8} s^{-1}) (Table 1). This trend may be relevant with the Marcus inverted region, which indicates the occurrence of incoherent ISF in Hc dimers according to the previous report.[25,32] Note that the singlet relaxation rate constants of Hc-ref (k_s: 6.0×10^{8} s^{-1}) and Pc-ref (k_s: 7.7×10^{7} s^{-1})[40] are much smaller than k_{TT} of *p*-$(Hc)_2$ and *p*-$(Pc)_2$, respectively (Table 1).

Table 1. Summarized Photophysical Parameters.

	k_{ISC}[a] (10^7/s^{-1}) [k_S[b] (10^7/s^{-1})]	k_{TT} (10^9 s^{-1})	k_{Diss}[j] (10^6 s^{-1})	k_{Rec}[k] (10^7 s^{-1})	k_T[l] (10^4 s^{-1})	η_{TT} (%)	η_T[n] (%)	A[p] (10^7 s^{-1})	$^{\circ}H^{\ddagger}$[q] (kJ·mol^{-1})	$^{\circ}S^{\ddagger}$[q] (J·mol^{-1}·K^{-1})	$-T\,^{\circ}S^{\ddagger}$ at 298 K[r] (kJ·mol^{-1})	$^{\circ}G^{\ddagger}$ at 298 K[s] (kJ·mol^{-1})
p-$(Hc)_2$	–	21[g]	16	52	12	100[m]	6 ± 2	2.4	0.303 ± 0.06	−109	32.5	32.8
m-$(Hc)_2$	–	0.45[g]	5.9	0.71	9.9	43[m]	39 ± 8	3.0	1.83 ± 0.06	−107	31.9	33.7
p-$(Pc)_2$	–	85[i]	4.7	4.8	3.3	100[i]	17[o]	4.0	2.55 ± 0.10	−105	31.3	33.8
m-$(Pc)_2$	–	2.1[h]	3.3[h]	0.26[h]	5.0[h]	94[h]	105[h]	4.9	5.62 ± 0.08	−101	30.1	35.7
Hc-ref	0.25[c] (60[d])	–	–	–	10	–	0.42 ± 0.22	–	–	–	–	–
Pc-ref	8.1[e] (7.7[f])	–	–	–	4.2[e]	–	16[e]	–	–	–	–	–

[a]k_{ISC}: Rate constant of ISC. [b]k_S: Deactivation rate constant of excited singlet state. [c]Estimated by psTA (Figure S17). [d]Estimated by fsTA (Figure S10). [e]Reported value.[41] [f]Reported value.[40] [g]Estimated by target analysis of fsTA. [h]Reported value.[10] [i]Reported value.[33] [j]Calculated by $k_{Diss} = (\Phi_1)^{-1} \times [\eta_T/(2\eta_{TT})]$. [k]Calculated by $k_{Rec} = (\Phi_1)^{-1} \times [(\eta_{TT} - \eta_T/2)/\eta_{TT}]$. [l]Calculated by $k_T = (\Phi_2)^{-1}$. [m]Calculated by $\eta_{TT} = k_{TT}/(k_{TT} + k_S)$. [n]Estimated by psTA (Tables S8-S10 in SI). [o]Estimated by psTA (Table S15 in SI). [p]Estimated by the Arrhenius plots (Figure S22 in SI). [q]Estimated by the

Eyring plots (Figure 3A). The standard errors in $^{o}S^{\ddagger}$ were less than ± 1 J·mol^{-1}·K^{-1} from the least square fittings. [r]Calculated by $-T\,^{o}S^{\ddagger} = -298\ (\mathrm{K}) \times {}^{o}S^{\ddagger}$. [s]Calculated by $^{o}G^{\ddagger} = {}^{o}H^{\ddagger} - T \times {}^{o}S^{\ddagger}$.

Then, to quantitatively discuss the dissociation process from TT to T_1+T_1, psTA spectra of Hc derivatives were measured (Figures S17-S18 in SI). In both Hc dimers, only T−T absorption signals at ca. 570 nm were observed in subnano- to micro-second time region. In contrast, two different lifetime components were clearly seen in the time-profiles. The slower component (k_T) was almost the same as T-T absorption of Hc-ref (Table 1, Figure S17 in SI). Therefore, the slower component can probably be attributed to the individual triplet states (T_1+T_1). Additionally, we also observed NIR region of *p*-$(Pc)_2$ and *p*-$(Hc)_2$ by using psTA (Figure S19 in SI). The broad absorption bands in the near-infrared region are deactivated with the same time constants as the first component of the T-T absorption decays. Therefore, these broad absorption bands can be attributed to the TT state. According to the recent report,[10] short and long lifetime components correspond to the correlated triplet pair (TT) and individual triplets (T_1+T_1), respectively. The individual triplet yields (Φ_T) can be estimated by utilizing the above mentioned Φ_{TT}. The Φ_T of *p*-$(Hc)_2$ and *m*-$(Hc)_2$ (maximum Φ_T: 200%) were accordingly determined to be 6 ± 2% and 39 ± 8%, respectively. Separately, the Φ_T of *p*-$(Pc)_2$ (17%) was calculated by using reported method (Figure S20 and Table S15 in SI).[10] The Φ_T of *m*-$(Pc)_2$ (105%) was employed as the reported value.[10] In both Hc and Pc dimers, the Φ_T of *p*-phenylene bridged dimers were smaller than those of *m*-phenylene bridged dimers (Table 1). These results can be probably attributed to the strong electronic coupling in *p*-phenylene bridged dimers.[10] Then, we also determined the rate constants of dissociation process from TT to T_1+T_1 (k_{Diss}) and recombination from TT to S_0 (k_{Rec}) by using bi-exponentially analysis of psTA (Table 1) considering the kinetic

processes as shown in Scheme 1A. The k_{Diss} values of Hc dimers are slightly larger than those of Pc dimers (Table 1). In contrast, the Φ_T of Hc dimers are much smaller than those of Pc dimers.

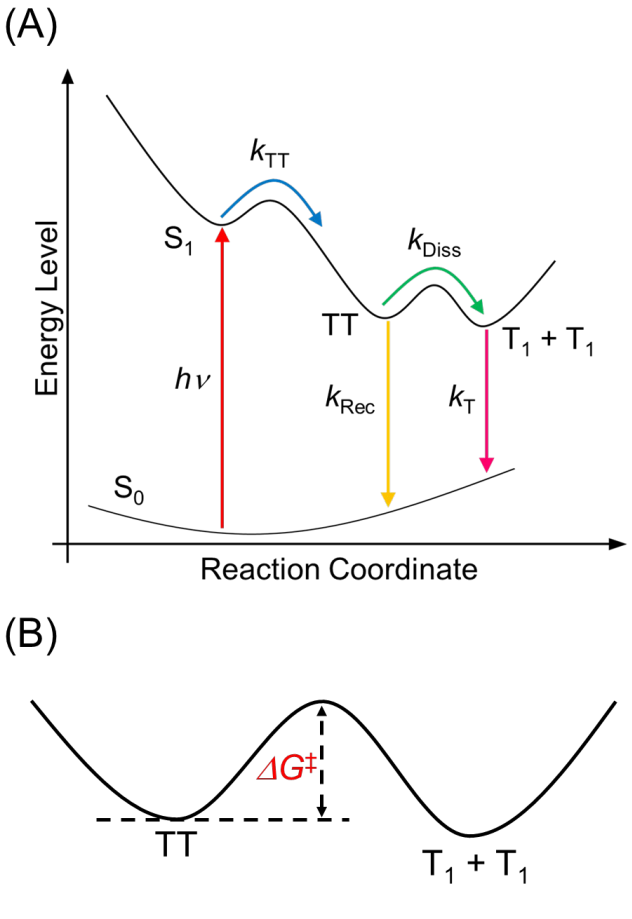

Scheme 1. (A) Potential energy surface on the kinetic processes in Hc and Pc dimers. (B) Enlarged potential surface forcusing the TT → T_1+T_1 dissociation with the activation free energy of $^{o}G^{\ddagger}$.

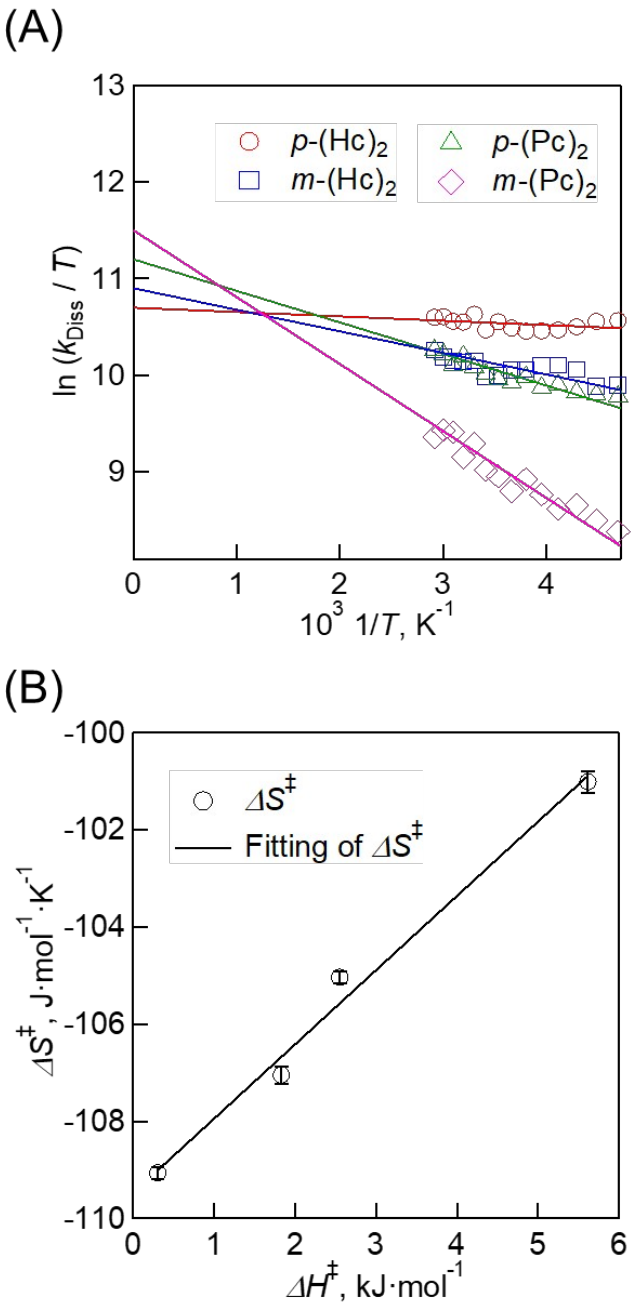

Figure 3. (A) Eyring plots of dissociation process in p-(Hc)$_2$, m-(Hc)$_2$, p-(Pc)$_2$ and m-(Pc)$_2$. The fitting function was calculated by the following equation: [ln (k_{Diss} / T) = – ($^{o}\bar{H}^{\ddagger}$ / RT) + ln (k_B / h) + ($^{o}\bar{S}^{\ddagger}$ / R)], where $^{o}\bar{H}^{\ddagger}$, R, h and $^{o}\bar{S}^{\ddagger}$ are activation enthalpy, gas constant, Planck constant and activation entropy, respectively. This panel well represent the enthalpy-entropy compensation effect because the intercept value is larger when the slope is larger. (B) Plots representing the enthalpy-entropy compensation ($^{o}\bar{S}^{\ddagger}$ vs. $^{o}\bar{H}^{\ddagger}$). The vertical error bars represent standard errors in $^{o}\bar{S}^{\ddagger}$ estimated from the least square fittings. The errors in $^{o}\bar{H}^{\ddagger}$ were less than 0.1 kJ·mol^{-1} as shown in Table 1.

To examine the reasons for the lower Φ_T of Hc dimers than those of Pc dimers, we further performed the temperature-dependent psTA measurements to estimate the parameters for the activation energy. We calculated pre-exponential factors (A) by using the Arrhenius plots of Hc and Pc dimers (Table 1 and Figures S21-S22 in SI). The values of A of Hc and Pc dimers are 2.4 × 10^7 s^{-1} for *p*-$(Hc)_2$, 3.0 × 10^7 s^{-1} for *m*-$(Hc)_2$, 4.0 × 10^7 s^{-1} for *p*-$(Pc)_2$ and 4.9 × 10^7 s^{-1} for *m*-$(Pc)_2$, respectively (Table 1). These different values of A and positive correlation between A and k_{Diss} in Hc and Pc dimers strongly suggest different vibrational role in these dimers. Next, we estimated the activation enthalpy ($^{o}H^{‡}$), activation entropy ($^{o}S^{‡}$) and Gibbs free energy of activation ($^{o}G^{‡}$) by Eyring plot (Figure 3A, Scheme 1B and Figure S21 in SI).[22,42,43] The detailed assumptions of Eyling plots is the activation entropy must be temperature independent. This assumption is satisfied by the fact that low frequency modes are mainly involved in promoting the various conformational motions.[37] The values of $^{o}H^{‡}$ of Hc and Pc dimers are 0.303 kJ·mol^{-1} for *p*-$(Hc)_2$, 1.83 kJ·mol^{-1} for *m*-$(Hc)_2$, 2.55 kJ·mol^{-1} for *p*-$(Pc)_2$ and 5.62 kJ·mol^{-1} for *m*-$(Pc)_2$, respectively (Table 1). The smaller $^{o}H^{‡}$ values of Hc dimers are probably attributable to the weaker electronic coupling of Hc dimers relative to Pc dimers (Figure S9 and Table S3 in SI). Then, the values of $^{o}S^{‡}$ of Hc and Pc dimers are −109 J·mol^{-1}·K^{-1} for *p*-$(Hc)_2$, −107 J·mol^{-1}·K^{-1} for *m*-$(Hc)_2$, −105 J·mol^{-1}·K^{-1} for *p*-$(Pc)_2$ and −101 J·mol^{-1}·K^{-1} for *m*-$(Pc)_2$, respectively (Table 1). Moreover, we successfully observed a good linear correlation between $^{o}H^{‡}$ and $^{o}S^{‡}$ resulted from enthalpy-entropy compensation effect (Figure 3B). To further evaluate the entropic contribution for $^{o}G^{‡}$, we calculated the values of $-T\,^{o}S^{‡}$ at 298 K. The values of $-T\,^{o}S^{‡}$ of Hc and Pc dimers are 32.5 kJ·mol^{-1} for *p*-$(Hc)_2$, 31.9 kJ·mol^{-1} for *m*-$(Hc)_2$, 31.3 kJ·mol^{-1} for *p*-$(Pc)_2$ and

30.1 kJ·mol^{-1} for *m*-(Pc)$_2$, respectively (Table 1). The emphasis is on the small differences of $-T\,^{o}S^{\ddagger}$ in both Hc and Pc dimers. Moreover, the values of $-T\,^{o}S^{\ddagger}$ are one or two orders of magnitude greater than that of $^{o}H^{\ddagger}$ in all systems. Based upon the transition state theory taking a low-frequency vibration mode with a frequency of ν ($h\nu \ll k_{B}T$) to derive the Eyring equation, these results indicate that the frequency factor determined by some specific vibration motions play a major role on the thermal activation ($^{o}H^{\ddagger} \approx RT$ from Table 1) of breaking the T-T binding enthalpy to weaken the electronic coupling, generating the T_1+T_1. To further examine the solvent viscosity and frozen matrix effects, additional psTA measurements were performed and we observed the slower decay processes of the TT state (Figures S23 and S24 in SI). The detailed discussions are described in SI. This is well consistent with the large degrees of intramolecular conformation changes by the low-frequency vibrations for the T_1+T_1 in *m*-(Pc)$_2$, *o*-(Pc)$_2$ and in *m*-(Hc)$_2$ (Table S13 in SI) concluded by the TREPR analyses of the spin-correlated triplet pairs.[37] Finally, we estimated the $^{o}G^{\ddagger}$ values at 298 K by using $^{o}H^{\ddagger}$ and $-T\,^{o}S^{\ddagger}$. The values of $^{o}G^{\ddagger}$ at 298 K of Hc and Pc dimers are 32.8 kJ·mol^{-1} for *p*-(Hc)$_2$, 33.7 kJ·mol^{-1} for *m*-(Hc)$_2$, 33.8 kJ·mol^{-1} for *p*-(Pc)$_2$ and 35.7 kJ·mol^{-1} for *m*-(Pc)$_2$, respectively (Table 1).

In contrast, the Φ_T values of Hc dimers are much smaller than those of Pc dimers as discussed in the above section. The plausible reason for the lower Φ_T values of Hc dimers is probably due to the lower energy levels of TT states than those of Pc dimers. Therefore, the direct recombination process from TT to S_0 is largely accelerated and the Φ_T values of Hc dimers decreased as compared to Pc dimers. The k_{Rec} values of Hc dimers are roughly an order of magnitude greater than those of Pc dimers. On the other hand, the large k_{Rec} values of *p*-phenylene bridged dimers relative to *m*-phenylene bridged dimers should be due to strong electronic couplings in *p*-phenylene bridged dimers (Figure S8 and Table S1 in SI). In Hc

dimers, the lower TT energy accordingly decelerated the ISF rates and accelerated the recombination rates from TT to S_0.

In conclusion, we demonstrated the synthesis and photophysical properties of Hc dimers with quantitative ISF by comparing with corresponding Pc dimers. The photophysical difference between Hc and Pc dimers lies in the triplet pair dissociation between Hc and Pc dimers, which results in the larger k_{Rec} values of Hc dimers than those of Pc dimers. Temperature-dependent transient absorption measurements demonstrated that the $^{o}H^{\ddagger}$ values of Hc dimers in the dissociation process are smaller than those of Pc dimers, whereas the relative entropic contributions ($-T^{o}S^{\ddagger}$) for $^{o}G^{\ddagger}$ are much larger than the enthalpic ones in both Hc and Pc dimers, implying that the vibration motions is responsible for the intramolecular conformation for weakening the electronic coupling in TT state to form the T_1+T_1 state. It is very interesting to note that there is no correlation between the dissociation yield Φ_T and the k_{Diss} values; $\Phi_T = 6 \pm 2\%$ is surprisingly low in *p*-$(Hc)_2$ despite the largest dissociation rate constants in Figure 3A. The dramatically small Φ_T values in the Hc dimers is ascribed to the smaller energy gaps between TT and S_0 relative to the gaps in the Pc dimers. Thus, the direct recombination process from TT to S_0 is largely accelerated in accordance with the energy-gap low for the nonradiative deactivation. The results associated with 'enthalpy-entropy compensation' provide a new perspective for the related research fields such as solar energy conversion, molecular electronics and quantum information science.[44,45]

ASSOCIATED CONTENT

Supporting Information

The supporting Information is available free of charge on the ACS Publications website at DOI: XXXX. Synthetic details, DFT calculations, absorption and fluorescence spectra, transient spectra, and detailed calculation processes.

AUTHOR INFORMATION

Corresponding Author

*E-mail: hasobe@chem.keio.ac.jp (T. H.).

*E-mail: nikolai.tkachenko@tuni.fi (N.T.).

*E-mail: ykobori@kitty.kobe-u.ac.jp (Y.K.).

ORCID

Taku Hasobe: 0000-0002-4728-9767

Nikolai V. Tkachenko: 0000-0002-8504-2335

Yasuhiro Kobori: 0000-0001-8370-9362

Notes

The authors declare no competing financial interest.

ACKNOWLEDGMENT

This work was partially supported by JSPS KAKENHI Grant Numbers of JP19H00888, JP20K21174 and Grant-in-Aid for Transformative Research Areas, “Dynamic Exciton” (JP20H05832) to Y.K. and by JSPS KAKENHI Grant Nos. JP18H01957, JP18K19063, JP20H05234, JP20KK0120 and JP21H01908 to T.H.. This work was partially carried out by the joint research program of Molecular Photoscience Research Center, Kobe University and the Research Program of "Five-star Alliance" in "NJRC Mater. & Dev."

REFERENCES

(1) Smith, M. B.; Michl, J. Singlet Fission. *Chem. Rev.* **2010**, *110*, 6891-6936.
(2) Miyata, K.; Conrad-Burton, F. S.; Geyer, F. L.; Zhu, X. Y. Triplet Pair States in Singlet Fission. *Chem. Rev.* **2019**, *119*, 4261-4292.
(3) Wasielewski, M. R. Dynamic Duos. *Nat. Phys.* **2017**, *13*, 114-115.
(4) Wilson, M. W. B.; Rao, A.; Clark, J.; Kumar, R. S. S.; Brida, D.; Cerullo, G.; Friend, R. H. Ultrafast Dynamics of Exciton Fission in Polycrystalline Pentacene. *J. Am. Chem. Soc.* **2011**, *133*, 11830-11833.
(5) Stern, H. L.; Cheminal, A.; Yost, S. R.; Broch, K.; Bayliss, S. L.; Chen, K.; Tabachnyk, M.; Thorley, K.; Greenham, N.; Hodgkiss, J. M., et al. Vibronically Coherent Ultrafast Triplet-Pair Formation and Subsequent Thermally Activated Dissociation Control Efficient Endothermic Singlet Fission. *Nat. Chem.* **2017**, *9*, 1205-1212.
(6) Lee, S.; Hwang, D.; Jung, S. I.; Kim, D. Electron Transfer from Triplet State of TIPS-Pentacene Generated by Singlet Fission Processes to $CH_3NH_3PbI_3$ Perovskite. *J. Phys. Chem. Lett.* **2017**, *8*, 884-888.
(7) Alagna, N.; Han, J.; Wollscheid, N.; Perez Lustres, J. L.; Herz, J.; Hahn, S.; Koser, S.; Paulus, F.; Bunz, U. H. F.; Dreuw, A., et al. Tailoring Ultrafast Singlet Fission by the Chemical Modification of Phenazinothiadiazoles. *J. Am. Chem. Soc.* **2019**, *141*, 8834-8845.
(8) Garoni, E.; Zirzlmeier, J.; Basel, B. S.; Hetzer, C.; Kamada, K.; Guldi, D. M.; Tykwinski, R. R. Two-Photon Absorption in Pentacene Dimers: The Importance of the Spacer Using Upconversion as an Indirect Route to Singlet Fission. *J. Am. Chem. Soc.* **2017**, *139*, 14017-14020.
(9) Sanders, S. N.; Kumarasamy, E.; Pun, A. B.; Trinh, M. T.; Choi, B.; Xia, J.; Taffet, E. J.; Low, J. Z.; Miller, J. R.; Roy, X., et al. Quantitative Intramolecular Singlet Fission in Bipentacenes. *J. Am. Chem. Soc.* **2015**, *137*, 8965-8972.
(10) Sakai, H.; Inaya, R.; Nagashima, H.; Nakamura, S.; Kobori, Y.; Tkachenko, N. V.; Hasobe, T. Multiexciton Dynamics Depending on Intramolecular Orientations in Pentacene Dimers:

Recombination and Dissociation of Correlated Triplet Pairs. *J. Phys. Chem. Lett.* **2018**, *9*, 3354-3360.
(11) Nakamura, S.; Sakai, H.; Nagashima, H.; Kobori, Y.; Tkachenko, N. V.; Hasobe, T. Quantitative Sequential Photoenergy Conversion Process from Singlet Fission to Intermolecular Two-Electron Transfers Utilizing Tetracene Dimer. *ACS Energy Lett.* **2019**, *4*, 26-31.
(12) Grieco, C.; Doucette, G. S.; Pensack, R. D.; Payne, M. M.; Rimshaw, A.; Scholes, G. D.; Anthony, J. E.; Asbury, J. B. Dynamic Exchange During Triplet Transport in Nanocrystalline TIPS-Pentacene Films. *J. Am. Chem. Soc.* **2016**, *138*, 16069-16080.
(13) Kato, D.; Sakai, H.; Tkachenko, N. V.; Hasobe, T. High-Yield Excited Triplet States in Pentacene Self-Assembled Monolayers on Gold Nanoparticles through Singlet Exciton Fission. *Angew. Chem. Int. Ed.* **2016**, *55*, 5230-5234.
(14) Pensack, R. D.; Tilley, A. J.; Grieco, C.; Purdum, G. E.; Ostroumov, E. E.; Granger, D. B.; Oblinsky, D. G.; Dean, J. C.; Doucette, G. S.; Asbury, J. B., et al. Striking the Right Balance of Intermolecular Coupling for High-Efficiency Singlet Fission. *Chem. Sci.* **2018**, *9*, 6240-6259.
(15) Tilley, A. J.; Pensack, R. D.; Kynaston, E. L.; Scholes, G. D.; Seferos, D. S. Singlet Fission in Core–Shell Micelles of End-Functionalized Polymers. *Chem. Mater.* **2018**, *30*, 4409-4421.
(16) Hasobe, T. Organic-Inorganic Hybrid Molecular Architectures Utilizing Self-Assembled Monolayers for Singlet Fission and Light Energy Conversion. *Chem. Lett.* **2021**, *50*, 615-622.
(17) Krishnapriya, K. C.; Musser, A. J.; Patil, S. Molecular Design Strategies for Efficient Intramolecular Singlet Exciton Fission. *ACS Energy Lett.* **2019**, *4*, 192-202.
(18) Gilligan, A. T.; Miller, E. G.; Sammakia, T.; Damrauer, N. H. Using Structurally Well-Defined Norbornyl-Bridged Acene Dimers to Map a Mechanistic Landscape for Correlated Triplet Formation in Singlet Fission. *J. Am. Chem. Soc.* **2019**, *141*, 5961-5971.
(19) Le, A. K.; Bender, J. A.; Arias, D. H.; Cotton, D. E.; Johnson, J. C.; Roberts, S. T. Singlet Fission Involves an Interplay between Energetic Driving Force and Electronic Coupling in Perylenediimide Films. *J. Am. Chem. Soc.* **2018**, *140*, 814-826.
(20) Inoue, Y.; Ikeda, H.; Kaneda, M.; Sumimura, T.; Everitt, S. R. L.; Wada, T. Entropy-Controlled Asymmetric Photochemistry: Switching of Product Chirality by Solvent. *J. Am. Chem. Soc.* **2000**, *122*, 406-407.
(21) Yeow, E. K. L.; Slep, L. D.; Chibisov, A. K.; Braslavsky, S. E. Photoinduced Electron-Transfer Reaction between the Erythrosin Dianion and $Mo(Cn)_8^{4-}$ in the Presence of Various Cations. The First Example of Enthalpy−Entropy Compensation in Electron Transfer between Anions. *J. Phys. Chem. A* **2003**, *107*, 439-446.
(22) Kitagawa, H.; Kobori, Y.; Yamanaka, M.; Yoza, K.; Kobayashi, K. Encapsulated-Guest Rotation in a Self-Assembled Heterocapsule Directed toward a Supramolecular Gyroscope. *Proc. Natl. Acad. Sci. U. S. A.* **2009**, *106*, 10444-10448.
(23) Chan, W.-L.; Ligges, M.; Zhu, X. Y. The Energy Barrier in Singlet Fission Can Be Overcome through Coherent Coupling and Entropic Gain. *Nat. Chem.* **2012**, *4*, 840-845.
(24) Dragan, A. I.; Read, C. M.; Crane-Robinson, C. Enthalpy–Entropy Compensation: The Role of Solvation. *Eur. Biophys. J.* **2017**, *46*, 301-308.
(25) Monahan, N. R.; Sun, D.; Tamura, H.; Williams, K. W.; Xu, B.; Zhong, Y.; Kumar, B.; Nuckolls, C.; Harutyunyan, A. R.; Chen, G., et al. Dynamics of the Triplet-Pair State Reveals the Likely Coexistence of Coherent and Incoherent Singlet Fission in Crystalline Hexacene. *Nat. Chem.* **2017**, *9*, 341-346.

(26) Bendikov, M.; Duong, H. M.; Starkey, K.; Houk, K. N.; Carter, E. A.; Wudl, F. Oligoacenes: Theoretical Prediction of Open-Shell Singlet Diradical Ground States. *J. Am. Chem. Soc.* **2004**, *126*, 7416-7417.
(27) Lukman, S.; Richter, J. M.; Yang, L.; Hu, P.; Wu, J.; Greenham, N. C.; Musser, A. J. Efficient Singlet Fission and Triplet-Pair Emission in a Family of Zethrene Diradicaloids. *J. Am. Chem. Soc.* **2017**, *139*, 18376-18385.
(28) Nakano, M.; Kishi, R.; Nitta, T.; Kubo, T.; Nakasuji, K.; Kamada, K.; Ohta, K.; Champagne, B.; Botek, E.; Yamaguchi, K. Second Hyperpolarizability (Γ) of Singlet Diradical System: Dependence of Γ on the Diradical Character. *J. Phys. Chem. A* **2005**, *109*, 885-891.
(29) Nakano, M.; Champagne, B.; Botek, E.; Ohta, K.; Kamada, K.; Kubo, T. Giant Electric Field Effect on the Second Hyperpolarizability of Symmetric Singlet Diradical Molecules. *J. Chem. Phys.* **2010**, *133*, 154302.
(30) Lee, J.; Bruzek, M. J.; Thompson, N. J.; Sfeir, M. Y.; Anthony, J. E.; Baldo, M. A. Singlet Exciton Fission in a Hexacene Derivative. *Adv. Mater.* **2013**, *25*, 1445-1448.
(31) Busby, E.; Berkelbach, T. C.; Kumar, B.; Chernikov, A.; Zhong, Y.; Hlaing, H.; Zhu, X. Y.; Heinz, T. F.; Hybertsen, M. S.; Sfeir, M. Y., et al. Multiphonon Relaxation Slows Singlet Fission in Crystalline Hexacene. *J. Am. Chem. Soc.* **2014**, *136*, 10654-10660.
(32) Sanders, S.; Kumarasamy, E.; Fallon, K. J.; Sfeir, M.; Campos, L. Singlet Fission in a Hexacene Dimer: Energetics Dictate Dynamics. *Chem. Sci.* **2020**, *11*, 1079-1084.
(33) Sakuma, T.; Sakai, H.; Araki, Y.; Mori, T.; Wada, T.; Tkachenko, N. V.; Hasobe, T. Long-Lived Triplet Excited States of Bent-Shaped Pentacene Dimers by Intramolecular Singlet Fission. *J. Phys. Chem. A* **2016**, *120*, 1867-1875.
(34) Purushothaman, B.; Parkin, S. R.; Anthony, J. E. Synthesis and Stability of Soluble Hexacenes. *Org. Lett.* **2010**, *12*, 2060-2063.
(35) Sanders, S. N.; Kumarasamy, E.; Pun, A. B.; Appavoo, K.; Steigerwald, M. L.; Campos, L. M.; Sfeir, M. Y. Exciton Correlations in Intramolecular Singlet Fission. *J. Am. Chem. Soc.* **2016**, *138*, 7289-7297.
(36) Abraham, V.; Mayhall, N. J. Simple Rule to Predict Boundedness of Multiexciton States in Covalently Linked Singlet-Fission Dimers. *J. Phys. Chem. Lett.* **2017**, *8*, 5472-5478.
(37) Kobori, Y.; Fuki, M.; Nakamura, S.; Hasobe, T. Geometries and Terahertz Motions Driving Quintet Multiexcitons and Ultimate Triplet–Triplet Dissociations via the Intramolecular Singlet Fissions. *J. Phys. Chem. B* **2020**, *124*, 9411-9419.
(38) van Stokkum, I. H. M.; Larsen, D. S.; van Grondelle, R. Global and Target Analysis of Time-Resolved Spectra. *Biochim. Biophys. Acta* **2004**, *1657*, 82-104.
(39) Snellenburg, J. J.; Laptenok, S.; Seger, R.; Mullen, K. M.; van Stokkum, I. H. M. Glotaran: A Java-Based Graphical User Interface for the R Package TIMP. *J. Stat. Softw.* **2012**, *49*, 1-22.
(40) Walker, B. J.; Musser, A. J.; Beljonne, D.; Friend, R. H. Singlet Exciton Fission in Solution. *Nat. Chem.* **2013**, *5*, 1019-1024.
(41) Zirzlmeier, J.; Lehnherr, D.; Coto, P. B.; Chernick, E. T.; Casillas, R.; Basel, B. S.; Thoss, M.; Tykwinski, R. R.; Guldi, D. M. Singlet Fission in Pentacene Dimers. *Proc. Natl. Acad. Sci. U. S. A.* **2015**, *112*, 5325-5330.
(42) Yong, C. K.; Musser, A. J.; Bayliss, S. L.; Lukman, S.; Tamura, H.; Bubnova, O.; Hallani, R. K.; Meneau, A.; Resel, R.; Maruyama, M., et al. The Entangled Triplet Pair State in Acene and Heteroacene Materials. *Nat. Commun.* **2017**, *8*, 15953.

(43) Lee, T. S.; Lin, Y. L.; Kim, H.; Pensack, R. D.; Rand, B. P.; Scholes, G. D. Triplet Energy Transfer Governs the Dissociation of the Correlated Triplet Pair in Exothermic Singlet Fission. *J. Phys. Chem. Lett.* **2018**, *9*, 4087-4095.
(44) Matsuda, S.; Oyama, S.; Kobori, Y. Electron Spin Polarization Generated by Transport of Singlet and Quintet Multiexcitons to Spin-Correlated Triplet Pairs During Singlet Fissions. *Chem. Sci.* **2020**, *11*, 2934-2942.
(45) Smyser, K. E.; Eaves, J. D. Singlet Fission for Quantum Information and Quantum Computing: The Parallel *JDE* Model. *Sci. Rep.* **2020**, *10*, 18480.